

# EMTP Model of Grid Connected PV System

Vijay K. Sood and Prabhpreet Bhalla

**Abstract** - Photovoltaic energy is one of the attractive candidates for green power generation. This paper investigates the connection of a solar photovoltaic (PV) system into an AC grid by modeling the system in Electromagnetics Transients Program (EMTP-RV). In this model, the popular single diode PV cell electrical model, based on the Shockley diode equation is used. Also, the two most commonly used Maximum Power Point Tracking techniques (MPPT), namely, Perturb and Observe (P&O) and Incremental Conductance (IC) are developed and compared. The direct control strategy employs a simple PI controller for the active/reactive power. However, it suffers from coupling of the two controllers and any change in one affects the other. Simulation results are presented to demonstrate the impact of sudden changes in atmospheric conditions and other disturbances on system performance. The simulation study performed shows that the system is robust against faults and other disturbances

**Keywords:** Direct Control, Pulse Width Modulation, Insulated Gate Bipolar Transistor, Coupled Watt-Var method, Voltage Source Inverter, Fast Fourier Transform

## I. INTRODUCTION

Studies have shown an exponential rise in the global solar PV market from \$2.5 billion in 2000 to \$71.2 billion in 2010 which corresponds to an annual growth rate of 39.5%. Power Electronics (PE) technology is increasingly being leveraged to integrate renewable and distributed generation (DG) systems. Recent developments in PE have resulted in enhanced control techniques for grid connected PV systems and have mitigated the negative effects of large penetration of PV systems on existing power systems [1, 6]. In this paper, such a system is modeled with the EMTP-RV simulation package.

The grid connected PV systems interface with the grid via a cascaded combination of DC/DC boost converter and DC/AC inverter. The boost converter steps up and regulates the DC voltage produced by the PV system so that the PV system can be interfaced to the inverter. Maximum power output from the array is achieved by MPPT techniques [2]. The algorithm systematically adjusts DC/DC converter switching and performs impedance matching until the maximum power point is found. The inverter then converts the fixed DC output voltage of the boost converter to AC and injects it into the grid at  $600V_{LL}$ .

The paper is organized in the following manner: Section II discusses the components that make up the grid-connected PV system briefly. Sections III and IV explain the simulated PV module and compare the MPPT techniques that are utilized to

extract maximum power from the PV module, respectively. Section V and VI discuss the 3-legged, 6-switch voltage source inverter (VSI) and its direct control strategy that controls the real power flow into the distribution network. Sections VII and VIII present the simulation results. The response to simulated disturbances such as changes in atmospheric conditions and various faults is investigated. Finally, conclusions and future work are discussed in section IX.

## II. SYSTEM DESCRIPTION

Fig. 1 shows the one-line diagram of the modelled system. The PV array consisting of 300 cells in series and 20 cells in parallel is used to obtain the required voltage and current output for conversion. The specifications of the simulated PV module are provided in Table.1 in the Appendix. The PV array output is fed to a DC/DC boost converter via a DC disconnect and fuse protection. The output of PV arrays is dependent on the level of solar irradiance and surface temperature. Therefore, the MPPT must be employed to operate the PV array around its MPP. The task of MPPT is to adjust DC/DC converter switch and match the load impedance to the ratio between voltage and current of the array at the MPP. The DC/DC converter outputs a DC voltage of  $600V_{dc}$  to feed into the 3-legged 6 switch voltage source inverter (VSI) which outputs  $600V_{LL}$ . A low-pass LC filter is employed to remove harmonics, before being fed to an isolation transformer to connect to the grid at the point of common coupling (PCC) via an AC disconnect switch, over-current fuse protection and AC Breaker panel.

## III. MODELING OF PV MODULE

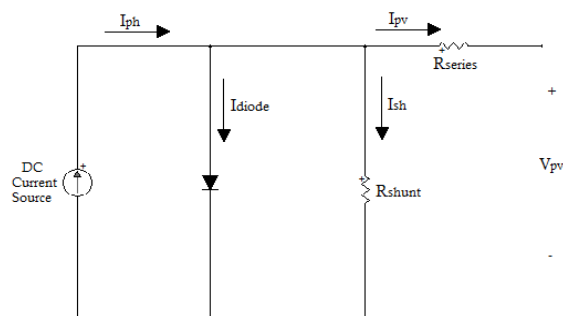


Fig 2: PV cell Model

The equivalent circuit of a PV cell is shown in Fig.2. It includes a current source, diode, series resistance and shunt resistance. A PV array is a group of several PV cells which are electrically connected in series and parallel circuits to generate the required current and voltage.

Authors are with the Faculty of Engineering and Applied Science, University of Ontario Institute of Technology (UOIT), Oshawa, Canada (e-mail: vijay.sood@uoit.ca)

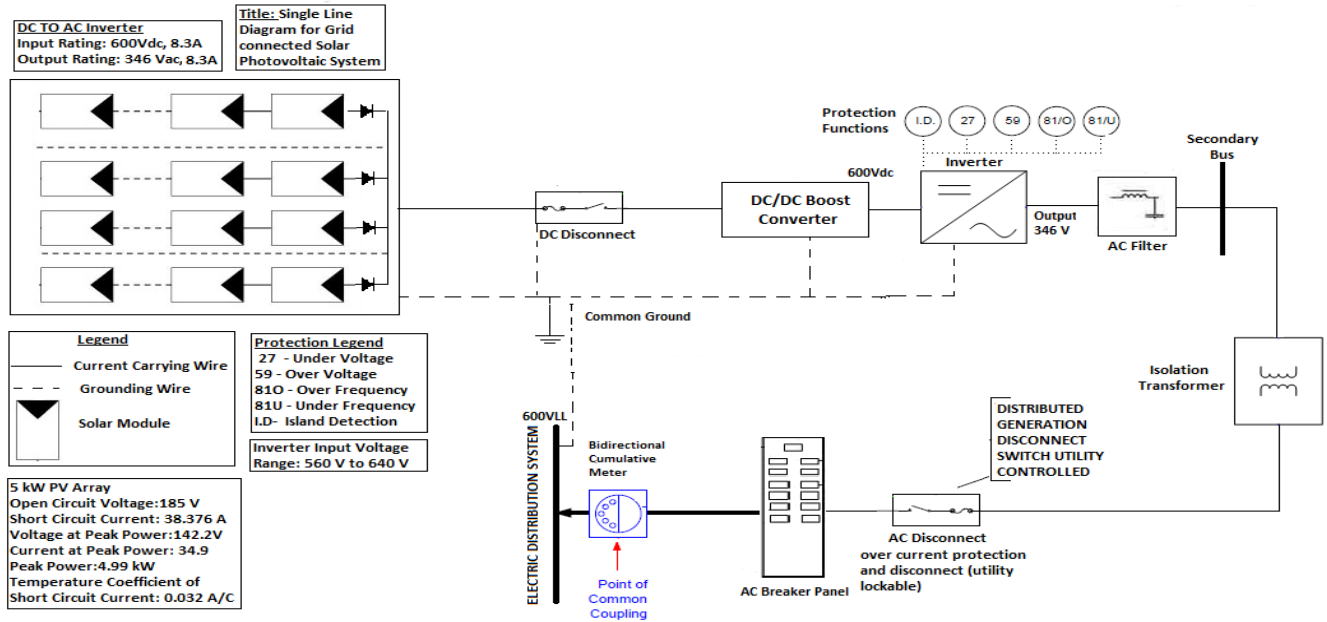


Fig 1: One Line Diagram

The following non-linear mathematical equation determines the relationship between voltage and current supplied by a PV module [7, 8, 9, 10].

$$I = N_p I_{PH} - N_p I_S \left[ \exp \left( \frac{q \left( \frac{V}{N_s} + I R_S \right)}{k T_C A} \right) - 1 \right] - \frac{\left( \frac{N_p V}{N_s} + I R_S \right)}{R_{SH}} \quad (1)$$

where  $I_{PH}$  is the light-generated current or photocurrent,  $I_S$  is the cell saturation of dark current,  $q = 1.6 \times 10^{-19}$  C is the electron charge,  $k = 1.38 \times 10^{-23}$  J/K is Boltzmann's constant,  $T_C$  is the cell's working temperature,  $A$  is diode's ideal factor,  $R_{SH}$  is the shunt resistance,  $R_S$  is the series resistance,  $N_p$  is the number of PV cells in parallel, and  $N_s$  is the number of PV cells in series.

The current,  $I_{PH}$  produced by the photoelectric effect can be calculated as follows

$$I_{PH} = [I_{SC} + K_I (T_C - T_{ref})] \lambda \quad (2)$$

where  $I_{SC}$  is the cell's short-circuit current at reference temperature: 25°C and reference irradiance: 1 kW/m<sup>2</sup>,  $K_I = 0.032$  is the cell's short-circuit current temperature coefficient,  $T_{ref}$  is the cell's reference temperature and  $\lambda$  is the solar insolation in kW/m<sup>2</sup>.

The cell's saturation current varies with the cell temperature, which is described as

$$I_S = I_{RS} \left( \frac{T_C}{T_{ref}} \right)^3 \exp \left[ \frac{q E_G \left( \frac{1}{T_{ref}} - \frac{1}{T_C} \right)}{k A} \right] \quad (3)$$

where  $I_{RS}$  is the cell's reverse saturation current at a reference temperature and irradiance, and  $E_G$  is the band energy of the semiconductor used in the cell.

The reverse saturation current at reference temperature can be approximately obtained as

$$I_{RS} = \frac{I_{SC}}{\left[ \exp \left( \frac{q V_{OC}}{N_s k T_C A} \right) - 1 \right]} \quad (4)$$

where  $V_{OC}$  is the cell's open circuit voltage.

To illustrate and verify the nonlinear  $I$ - $V$  characteristics of the PV array, model was simulated for different irradiance and temperature.

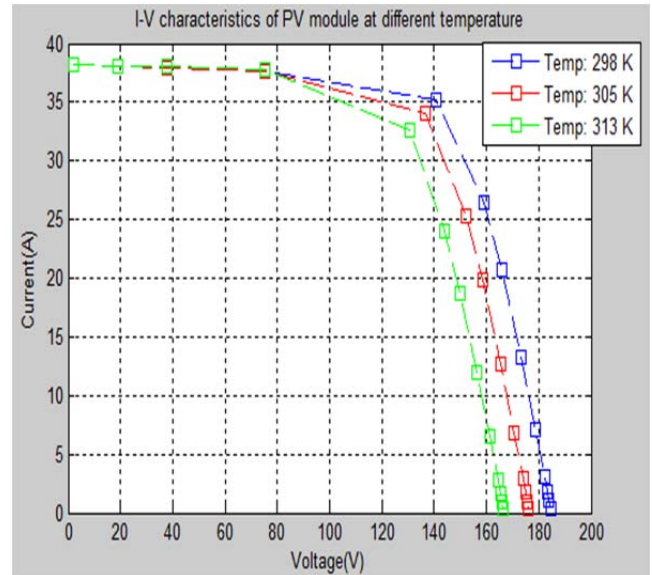


Fig. 3:  $I$ - $V$  Characteristics of PV module with varying cell temperature

Fig. 3 shows the  $I$ - $V$  characteristics with the variation in temperature level at a constant solar irradiance of 1000W/m<sup>2</sup>. It can be seen that the  $I$ - $V$  curve shift to the right and open circuit voltage reduces with the increase in temperature, while there is a very little change in short circuit current.

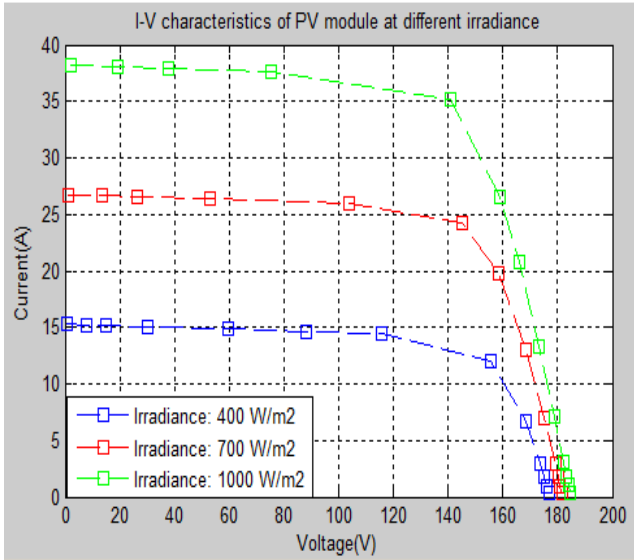


Fig. 4: *I-V* Characteristics of PV module with varying irradiance

Fig.4 shows the effect of the change in solar irradiance level at constant cell temperature of 25°C on *I-V* characteristics of the PV module. It can be seen that the short circuit current increases with increase in insolation level, while there is very little change in the open-circuit voltage.

#### IV. MAXIMUM POWER POINT TRACKING (MPPT)

The two most commonly used MPPT techniques, namely, Perturb and Observe (P&O) and Incremental Conductance (IC) were developed and compared in EMTP. The aim is to perform impedance matching by controlling the PV array's output voltage by controlling the duty cycle of the DC/DC Boost Converter switch [3].

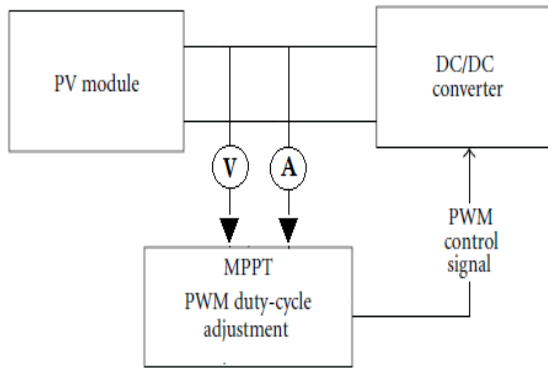


Fig. 5: Maximum Power Extraction Operation

Both algorithms have their own advantages and disadvantages but P&O algorithm was used in the simulation of the complete system since it can be easily implemented by digital circuits.

##### A. Perturb and Observe (P&O) Algorithm

P&O algorithm is widely used in PV systems. It operates by continuously perturbing the PV array's terminal voltage

and comparing the output power with that of the previous perturbation. The P&O operation flowchart is shown in Fig. 6.

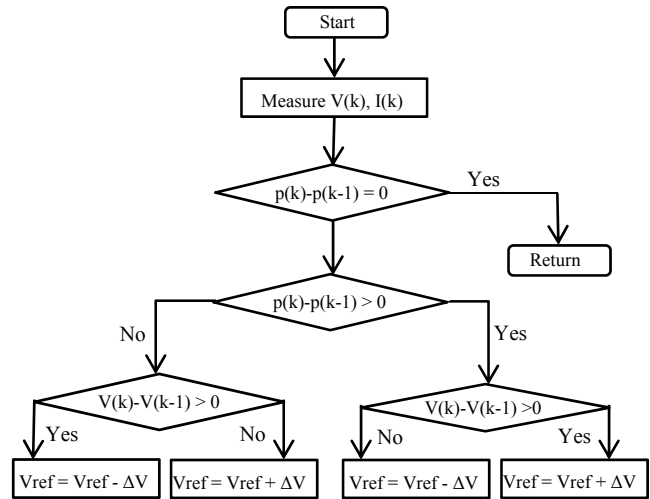


Fig. 6: P&O Operation Flowchart

If the output power increases with the perturbation, the algorithm continues in the same direction, otherwise the terminal voltage is perturbed in the reverse direction. Once the MPP is reached, the operating point oscillates around it. The tracking speed and the oscillations depend on the perturbation size and perturbation cycle. The tracking speed increases as the perturbation size is increased. However, the amplitude of the oscillations also gets larger resulting in power loss.

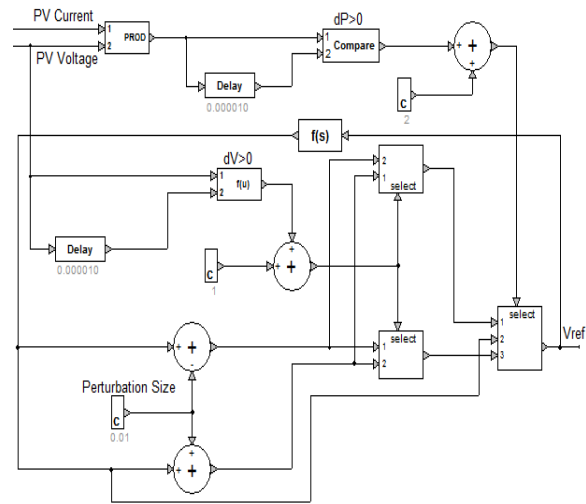


Fig. 7: P&O Operation implementation

The P&O algorithm (Fig. 7) starts its cycle by measuring the present array terminal voltage and current. The power is then calculated and compared with power at the end of a preceding perturbation cycle using the 'delay' block in EMTP. The perturbation size and cycle used in the simulation are 0.01 V and 10 us, respectively. The algorithm then carries out the  $dP > 0$  test. According to the result of this check, the algorithm performs the control action using the 'select' block to perturb the array terminal voltage.

## B. Incremental Conductance Algorithm

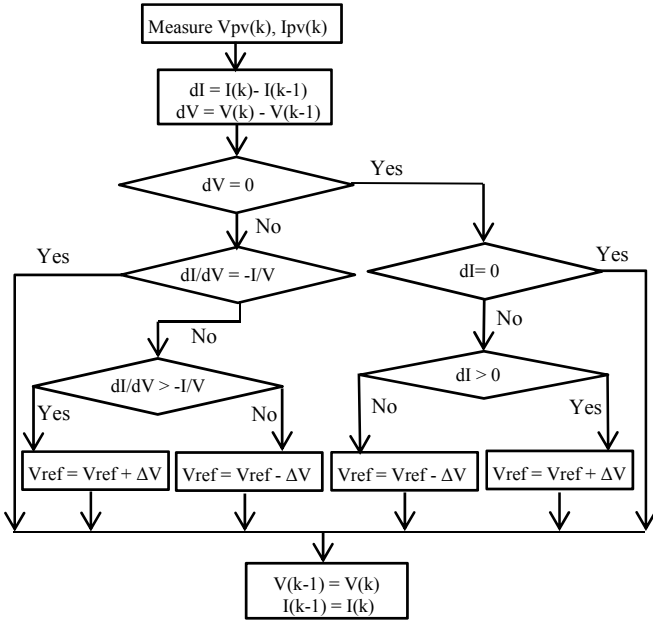


Fig. 8: IC Operation Flowchart

IC algorithm (Fig.8) can overcome some of the drawbacks of P&O algorithm but its implementation is more complex. The IC algorithm is based on the fact that at the MPP, the derivative of the power with respect to the voltage is zero.

$$\frac{dP}{dV} = 0 \text{ at the MPP}$$

$$\frac{dP}{dV} > 0 \text{ on the left side of the MPP}$$

$$\frac{dP}{dV} < 0 \text{ on the right side of the MPP}$$

$$\frac{dP}{dV} = I + \left(\frac{dI}{dV}\right) * V \quad (5)$$

$$\text{At MPP, } I = - \left(\frac{dI}{dV}\right) * V \quad (6)$$

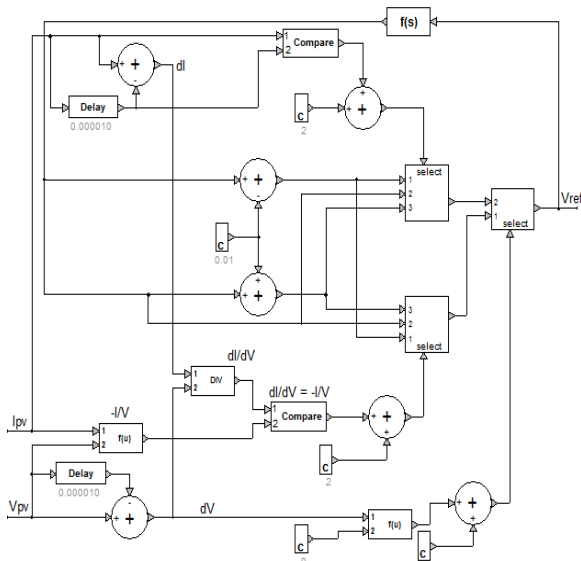


Fig. 9: IC Algorithm Implementation

The IC algorithm implementation (Fig. 9) starts its cycle by measuring the instantaneous current and voltage values, and then calculates the incremental values,  $dI$  and  $dV$  using the 'delay' blocks in EMTP as show in Fig. 9. The algorithm carries out the main check by comparing the  $dI/dV$  against  $-I/V$ . Using the 'select' block in EMTP, the reference voltage ( $V_{ref}$ ) provided to the MPPT converter is adjusted based on this check and equations (5)-(6). If  $dI/dV = -I/V$ , then the algorithm does not change the  $V_{ref}$  and the adjustment stage is bypassed. The algorithm performs  $dV=0$  check before the main check to determine whether the system is already operating at the MPP in the preceding cycle ( $dV=0$ ). If  $dV=0$ , then the algorithm bypasses the main check,  $dI/dV = -I/V$  entirely and instead checks if  $dI=0$  to determine whether the atmospheric conditions have changed. If change is detected, the algorithm once again utilizes the 'select' block and adjusts the  $V_{ref}$  depending on whether  $dI$  is positive or negative.

## V. VOLTAGE SOURCE INVERTER

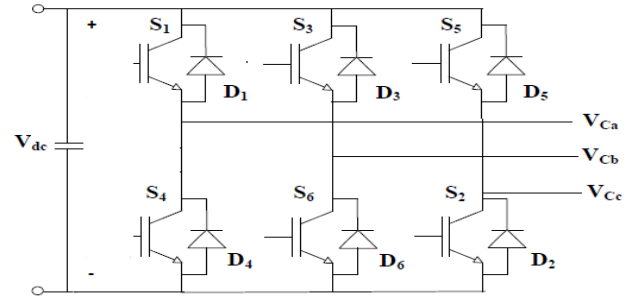


Fig. 10: Voltage Source Inverter

The 3-legged, 6-switch DC to AC inverter (Fig.10) takes 6 signal inputs that are fed to the switches. The sub-circuit block on each leg of the DC to AC inverter is a combination of a switch, inverse connected diode and a RC snubber.

A capacitor connected on the DC side of the VSI acts as a DC voltage source. The IGBT based VSI uses Pulse-Width Modulation (PWM) technique to synthesize a sinusoidal waveform from a DC voltage. The 60 Hz sinusoidal waveform is synthesized by a technique called unipolar voltage switching. Harmonics are cancelled by connecting an LC filter with corner frequency of 120 Hz at the AC side of the VSI.

## VI. VSI CONTROL STRATEGY

The steady state active power  $P$  and reactive power  $Q$  flowing between the PV System and AC system is given by

$$P = \frac{V_{grid} * V_{inv} \sin(\delta)}{X_S} \quad (7)$$

$$Q = \left(\frac{V_{grid}^2}{X_S}\right) (V_{inv} \cos(\delta) - V_{grid}) \quad (8)$$

where  $V_{grid}$  is AC system voltage,  $V_{inv}$  is the inverter's output voltage,  $\delta$  is phase angle between  $V_{grid}$  and  $V_{inv}$ , and  $X_S$  is the transformer reactance.

From the above equations, it can be seen that the active power provided by the inverter depends on transmission angle,  $\delta$  and magnitude of inverter's output voltage. The AC system voltage can be considered as constant in case of strong AC system. The only input to the converter is gate pulses to the converter valves. By controlling the phase shift of PWM pulses, the active power injected into the network can be controlled. This method is also called coupled Watt-Var or  $P$ - $Q$  method because the active and reactive powers are coupled and any change in one affects the other.

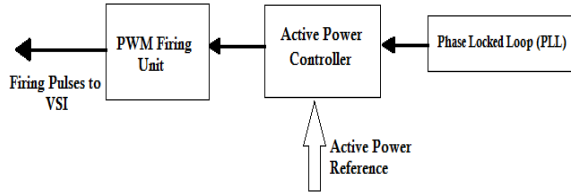


Fig. 11: Inverter's Control System

A Phase Locked Loop (PLL) [6] is utilised to lock on the grid frequency and provide a stable reference synchronization signal for the firing unit (Fig.11). The inverter's control strategy maintains the power exchange with the network [5]. System parameters are provided in Table 2 in the Appendix.

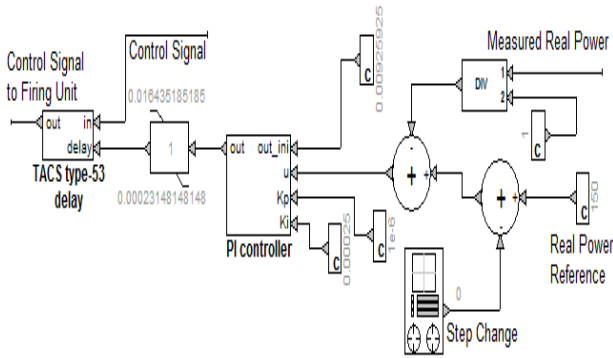


Fig. 12: Watt-Var PI Controller

The controller measures the real power being injected into the grid and employs a PI controller (Fig.12) to control the phase shift of the reference synchronization signal for the firing unit. This simpler method was employed since the main focus of the paper was the implementation of the MPPT blocks in EMTF. This method is now obsolete as it suffers from coupling of the real and reactive powers. However, a system with a decoupled control method based on the d-q transformation theory which allows for independent control of watts and Vars is being implemented in EMTF in the future.

## VII. SIMULATION RESULTS

### A. Step Change in Temperature (Fig.13)

In this study, a step change was imposed in the operating temperature of the PV module. At the beginning of the simulation, the temperature is set to 298° K. At 0.25s, a step change of 15° K was imposed.

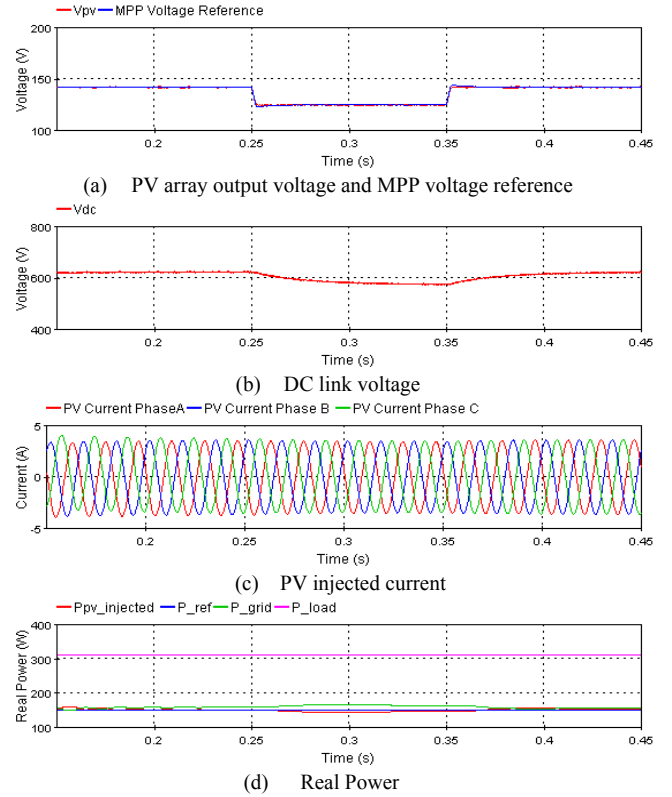
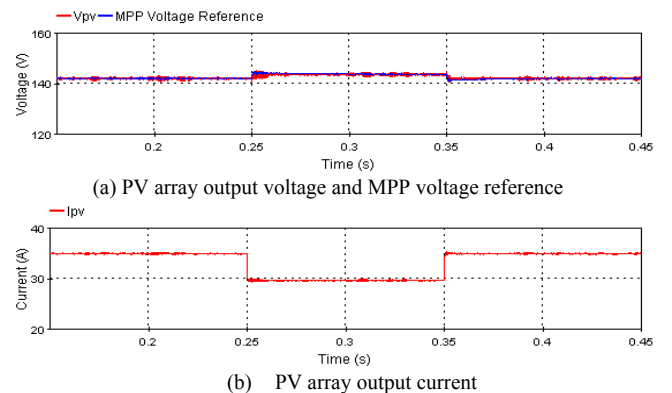


Fig. 13: Step Change in Temperature

Fig. 13 shows that MPP voltage reduces as  $I$ - $V$  curve shifts to the right with the increase in temperature, while there is a very little change in short circuit current. The DC link voltage also drops as a result of the change in input voltage. The current injected into the network is shown in Fig.13(c). A FFT of the current waveform showed the presence of 7<sup>th</sup> harmonics. Since the load is purely resistive, the reactive power consumed by it is zero. In Fig. 13(d), it can be seen that the load requires 300 W; of which 150 W are delivered by the PV system. The remaining real power demand is supplied by the utility. Ripples in the Real power are due to the 5<sup>th</sup>, 7<sup>th</sup> and 11<sup>th</sup> harmonics present in the Bus Voltage.

### B. Step Change in Irradiance (Fig.14)

At the beginning of the simulation, the irradiance is set to 1 kW/m<sup>2</sup>. At 0.25s, a step change of 0.15 kW/m<sup>2</sup> was imposed. The system response is shown in Fig. 14.



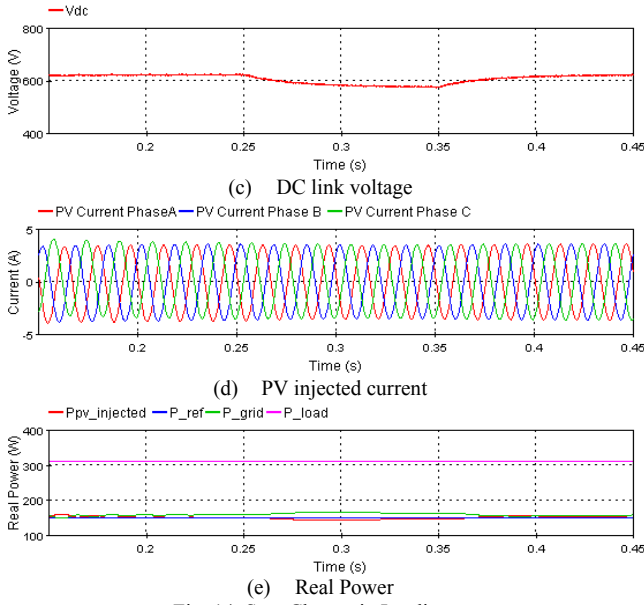


Fig. 14: Step Change in Irradiance

It can be seen in Fig. 14(a) that there is very little change in the PV module's output voltage. PV array current is heavily dependent on the irradiance. It drops to 29.3 A from its initial value of 34.1 A. This causes the maximum theoretical power to drop to 4.25 kW. The DC link voltage also drops but stays within the 10% limit. The current injected into the network are shown in Fig 14(c). The control strategy maintains the active power at a constant value. Therefore, the PV system's operation remains stable as the irradiance changes.

### C. Step Change in Active Power demand (Fig.15)

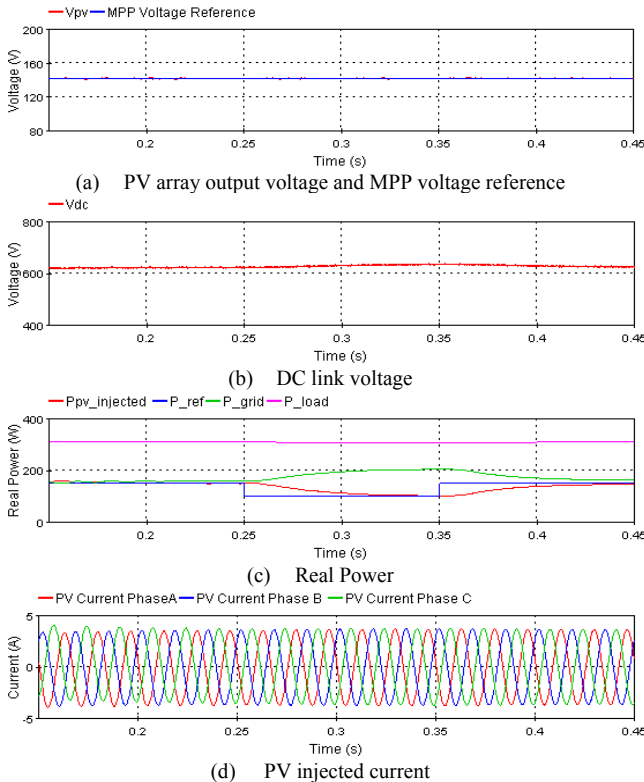


Fig. 15: Step Change in Active Power Demand

Fig. 15(c) shows that the power injected into the network follows the reference power commands with considerable accuracy. It can also be seen that the slight change in the bus voltage causes a slight dip in the power consumed by the load. The DC link voltage is robust against step change in power command as shown in Fig. 15(b).

## VIII. FAULT ANALYSIS

The operation of the distribution system's protective relays can be interrupted by the distributed generation systems. For instance – if a DG system is connected between the substation and the point of fault location, it will contribute to the fault current. It could result in an under reach situation and the protection relay would not be able to detect the fault. Therefore, it is very important to study the behavior of DG systems under fault conditions.

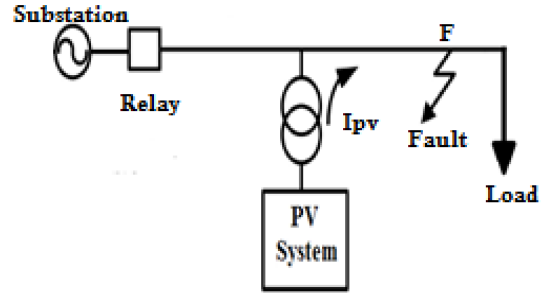


Fig. 16: Fault Location

### A. Single Line to Ground fault

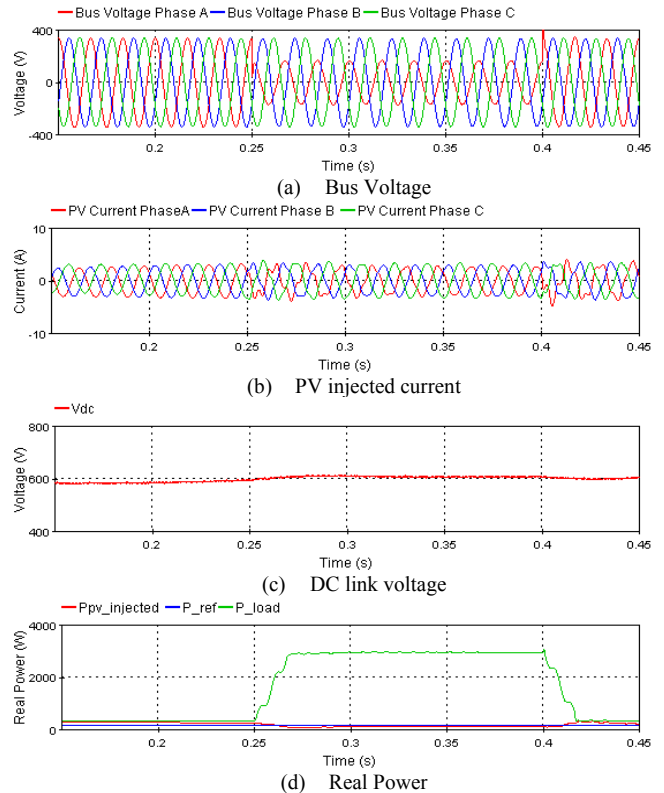


Fig. 17: Single Line to Ground Fault

A single phase to ground fault is simulated at location F shown in Fig. 16. The fault occurs at 0.25s and is cleared at 0.4s. The fault results in reduction of the phase A bus voltage, also known as voltage sag. The phases B and C voltages remain at their nominal values. The injected current does not increase and makes no contribution to the fault current. It can be seen in Fig. 17(c) that the boost converter's output voltage increases but then stabilizes at a value equal to the one before the fault. In response to sag in primary bus voltage, the DC-AC inverter's control system adjusts its output in order to maintain the required real power flow. The real power supplied by the PV system is shown in Fig. 17(d).

### B. Three Phase to Ground fault (Fig.18)

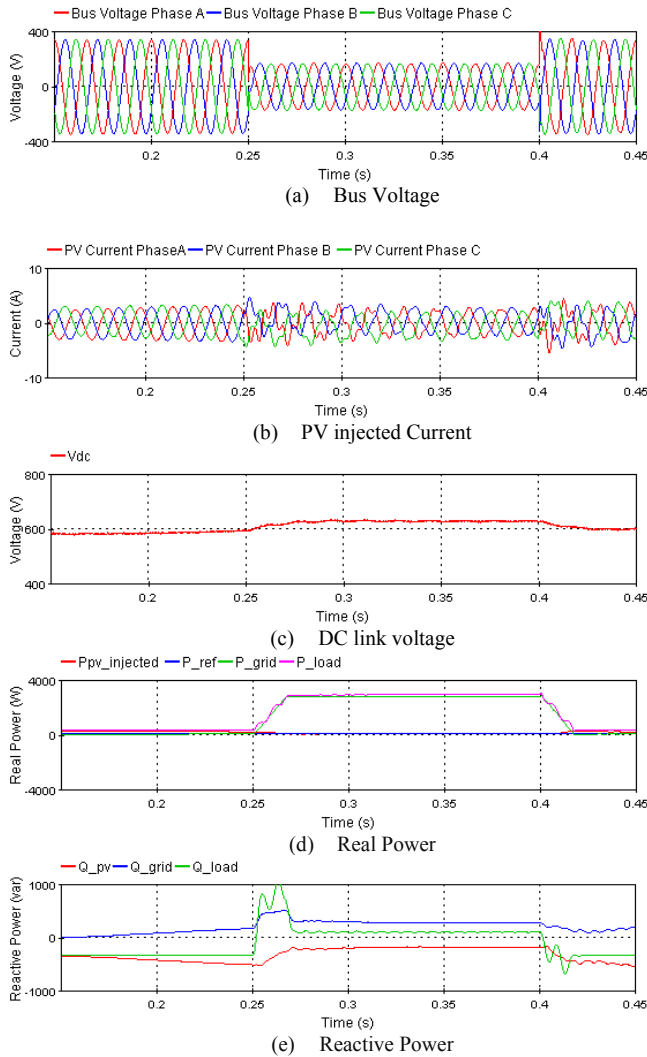


Fig. 18: Three Phase to Ground Fault

A three phase to ground fault is simulated at location F shown in Fig. 16. The fault occurs at 0.25s and is cleared at 0.4s. It causes a voltage dip in all 3 phase voltages. To regulate the boost converter's input voltage, the controller performs impedance matching which causes the DC link voltage to increase up to 625 V as shown in Fig. 18(c). The voltage stabilizes at 620V within 0.1s. The transients in the injected sinusoidal AC currents shown in Fig. 18(b) take about 0.08s to mitigate. The injected current by the PV system does

not increase and makes no contribution to the load current as in the case of single phase to ground fault. The real power injected into the grid is shown in Fig. 18(d). The real power controller regulates the real power injected to a constant value equal to the one before the fault. In Fig. 18(e), it is evident that when the fault occurs, the reactive power consumed by the load also suffers from transients. The transients damp out in less than two cycles.

## IX. CONCLUSION

In this paper, the control and interfacing of a PV generation system with utility grid is investigated. The MPPT keeps the PV array operating at the optimum point under changing atmospheric conditions and the DC/DC boost converter's output voltage stays within the 10% limit. The control strategy maintains the active power at a constant value in case a step change in active power demand is imposed. However, as the results show the active and reactive power are coupled and any change in one affects the other. The PV system showed good performance under fault conditions. The operation remains stable and no contribution to the fault current was made by the PV system. It is beneficial as the protection equipment ratings or even settings would not have to be changed to accommodate PV systems.

## X. APPENDIX

Table 1: PV Module Specifications

Characteristics	Specification
Open circuit voltage	185 V
Short circuit current	38.376 A
Voltage at peak power	142.2 V
Current at peak power	34.9 A
Peak Power	4.96 kW
Temperature co-efficient of short circuit current	0.032A/°C
Series Resistance, $R_S$	0.604 ohms
Shunt Resistance, $R_{SH}$	140 ohms

Table 2: Parameters of the System

Parameter	Specification
Switching Frequency for PWM	540 Hz
Power System Rating	5kVA
DC Voltage	600±40V
Proportional gain for power controller, $k_p$	1e-6
Integral gain for power controller, $k_i$	0.00025

## XI. REFERENCES

- [1] W. Kramer *et al.*, "Advanced Power Electronic Interfaces for Distributed Energy Systems Part 2: Modeling, Development, and Experimental evaluation of Advanced Control Functions for Single-Phase Utility Connected Inverter," National Renewable Energy Laboratory, Golden, Colorado, NREL/TP-550-44313, Nov. 2008.

- [2] Kinal Kachhiya et al., "Matab/ Simulink model of solar PV module and MPPT algorithm" in National Conf. on Recent Trends in Engineering & Technology," 2011.
- [3] B. M Hasaneen and Adel A. Elbaset, "Design and simulation of DC/DC boost converter," in The 12th International Middle East Power System Conf., MEPCON'2008, South Valley University, Faculty of Eng., Aswan, Egypt, Vol. I, March 13-15, 2008
- [4] Ahmed Said Khalifa, "Control and interfacing of three phase grid connected photovoltaic systems," MASc thesis. Dept. Elect. and Computer Eng., Univ. of Waterloo, Waterloo, Ontario, Canada, 2010.
- [5] Charan Langton. "Unlocking the Phase Locked Loop - Part 1," [Online]. Available: <http://www.complextoreal.com>.
- [6] Yun Tiam Tan, "Impact on the Power System with a Large Penetration of Photovoltaic Generation," Ph.D. dissertation. Dept. of Electrical Engineering and Electronics. The University Of Manchester Institute Of Science and Technology, Manchester, England, 2004.
- [7] Sonal Panwar and R.P Saini, "Development and Simulation of Solar Photovoltaic model using Matlab/simulink and its parameter extraction," in International Conf. on Computing and Control Engineering, 2012 © Coimbatore Institute of Information Technology.
- [8] Natarajan Pandiarajan et al., "Application of Circuit Model for Photovoltaic Energy Conversion System". International Journal of Photoenergy, Vol. 2012, No.410401, Nov., 2011.
- [9] J.A Ramos-Hernanz et al., "Two Photovoltaic Cell Simulation Models in Matlab/Simulink". International Journal on Technical and Physical Problems of Engineering, Vol. 4, No. 1, pp. 45-51, March, 2012.
- [10] Villalva, M.G.; Gazoli, J.R.; Filho, E.R., "Comprehensive Approach to Modeling and Simulation of Photovoltaic Arrays," IEEE Transactions on Power Electronics, Vol: 24, Issue: 5, 2009, Page(s): 1198 - 1208